



UvA-DARE (Digital Academic Repository)

Structured doping of upconversion nanosystems for biological applications

Wang, Y.

Publication date
2011

[Link to publication](#)

Citation for published version (APA):

Wang, Y. (2011). *Structured doping of upconversion nanosystems for biological applications*. [Thesis, fully internal, Universiteit van Amsterdam].

General rights

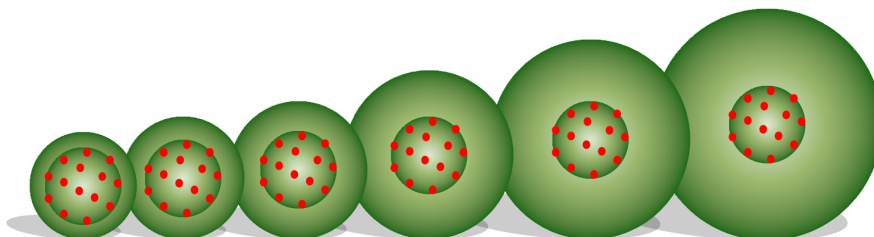
It is not permitted to download or to forward/distribute the text or part of it without the consent of the author(s) and/or copyright holder(s), other than for strictly personal, individual use, unless the work is under an open content license (like Creative Commons).

Disclaimer/Complaints regulations

If you believe that digital publication of certain material infringes any of your rights or (privacy) interests, please let the Library know, stating your reasons. In case of a legitimate complaint, the Library will make the material inaccessible and/or remove it from the website. Please Ask the Library: <https://uba.uva.nl/en/contact>, or a letter to: Library of the University of Amsterdam, Secretariat, P.O. Box 19185, 1000 GD Amsterdam, The Netherlands. You will be contacted as soon as possible.

CHAPTER 3

Effect of Surface-Related Organic Vibrational Modes in Luminescent Upconversion Dynamics of Rare Earth Ions Doped Nanoparticles



Chapter 3

Abstract: The surface of nanoparticles is known to be of large importance for determining the physical and chemical properties of nanoparticles. For their biological/biomedical applications the surface of the nanoparticles has to be modified which inevitably affects their performance. In this work we have studied the effects of the surface-related organic vibrational modes on the spectroscopic properties of rare earth ions in one of the most efficient luminescence upconversion nanosystems - NaYF₄. Specifically, the effects of the surface quench centers, the surface-related luminescent centers, as well as the role of shell properties have been investigated spectroscopically. Our results demonstrate that the surface-related high-frequency vibrational modes can be critical for the spectral properties of the nanosystems once the surface is not well separated from the discrete luminescent centers.

Keywords: upconversion • nanoparticle • surface • core/shell structure • vibrational mode

3.1 Introduction

Surface interactions between inorganic nanoparticles and organic molecules, as well as their effects on the physical and chemical properties of the nanoparticles are key to the application of nanomaterials, especially in the biological and biomedical field. Upconversion nanoparticles (UCNPs), typically rare earth ions doped ones (e.g. NaYF₄^[1]), are considered as being of great potential as fluorescence labels for applications such as imaging, therapy and detection.^[2] Their unique advantages include the virtual absence of photobleaching, multicolor labeling, deep penetration of (NIR) excitation light in human tissues and the fact that upconversion can simply be induced by a continuous wave (CW) diode laser. In recent years several approaches have been taken to improve the upconversion efficiency. These approaches addressed host material, lattice structure, doping concentration and vibrational energy of surface ligands, *etc.*. Lower symmetry and lower phonon energy of the crystal lattice are beneficial for the upconversion emission since vibrational coupling with the transition of rare earth ions can enhance the non-radiative relaxation. Sensitizer-acceptor co-doped upconversion material is considered to be a good choice and the Yb³⁺ ion is usually taken as a good sensitizer for upconversion, as it has a large absorption cross section for NIR irradiation and a proper energy level scheme for efficient energy transfer to Er³⁺/Tm³⁺ ions.

To study the effect of the surface-related organic vibrational modes on the spectroscopic properties of rare earth ions in upconversion nanoparticles, we have designed a series of core/shell nanoparticles with a varying thickness of the homogeneous shell. Coating with a homogeneous shell outside a core is considered as an efficient route to improve the luminescence properties of upconversion nanoparticles.^[3] In general it is thought to be able either to modify/minimize the surface defects and/or to shield high-frequency vibrating bonds from the outside. In this work we focus on the influence of the shell thickness of α -NaYF₄:Yb³⁺,Er³⁺@ α -NaYF₄ on the upconversion dynamics, and elucidate the role of a homogeneous coating.

3.2 Experiments

3.2.1 Chemicals

Rare earth oxides (RE = Y, Yb, Er), oleylamine (OM, >80%, *Acros*), oleic acid (OA, 90%), octadecene (ODE, 90%, *Acros*), trifluoroacetic acid (99%, *Acros*), CF₃COONa

Chapter 3

(>97%, Acros), 2-aminoethyl dihydrogenphosphate (AEP) was purchased from *Aldrich*. Ethanol, chloroform and hexane of analytical grade were purchased from *Beijing Chemicals* and used without further purification. Water used in the experiment was purified to a resistivity of 18.2M Ω .

3.2.2 Synthesis of NaYF₄:Yb³⁺,Er³⁺@NaYF₄ core/shell structured upconversion nanoparticle

The synthesis of nanoparticles followed a similar scheme as reported before.^[4] Briefly, rare earth trifluoroacetates (CF₃COO)₃RE·3H₂O were prepared by dissolving relative rare earth oxides in trifluoroacetic acid, followed by drying at 60 °C. A mixture of designated molar ratio of trifluoroacetate salts powder (Na⁺/RE³⁺ = 1/1, Y³⁺/Yb³⁺/Er³⁺ = 78/20/2, mol/mol) was dissolved in 10 mL oleic acid (OA), 10 ml oleylamine (OM) and 20 mL octadecene (ODE), and then passed through a filter to get rid of the residues. Under vigorous stirring in a three-neck flask, the mixture was heated to 110 °C under vacuum and maintained at this temperature to remove the residual water and oxygen for more than 30 min during which time the flask was purged periodically with dry argon gas for protection from oxidation. At this point the solution was totally clear with a slight orange color. Subsequently, the mixture was heated slowly to 250 °C under argon atmosphere conditions. After 2 hours, all the products were cooled to room temperature and separated into six equal parts. Every part of the product we obtained was reheated to 250 °C under vigorous stirring and under dry argon gas conditions, after which different amounts of shell precursors solutions containing equal molar of sodium trifluoroacetate and yttrium trifluoroacetate were slowly added into the reaction systems. All of the followed reactions were allowed to continue for another 1 hour. Every final mixture was cooled down rapidly to room temperature, precipitated with ethanol, and isolated via centrifugation for at least three times. The resulting nanocrystals were dried in vacuum at 60 °C for a minimum of 24 hours. According to the increasing amount of shell materials we added, the samples were marked as **S1**, **S2**, **S3**, **S4**, **S5** and **S6** (see also **Scheme 3.1**).

3.2.3 Phase transfer of upconversion nanoparticle from hydrophobic to hydrophilic

The AEP ligand surface UCNPs were obtained via a ligand exchange process by 2-aminoethyl dihydrogenphosphate (AEP). 200 mg of AEP was dispersed into a 10 ml mixture of water and ethanol (volume ratio is 3:2). The hydrophobic UCNPs solution (~20 mg, purified and dispersed in 5 mL of chloroform) were mixed with the AEP solution and stirred vigorously over 48 hours at 30 °C. The UCNPs transferred from the bottom chloroform layer to the top H₂O/CH₃CH₂OH layer, which was collected and washed three

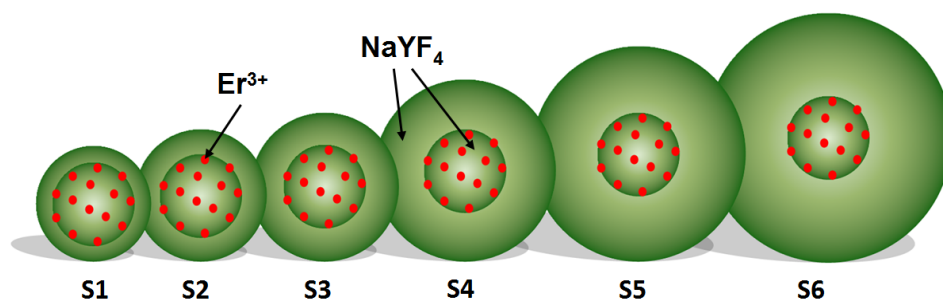
times by water. After centrifugation, the obtained nanoparticles were redispersed in water. After phase transfer, the AEP-terminated UCNPs provide an amino group which can be used for covalently coupling with carboxyl-terminated molecules.

3.2.4 Characterizations

Structure characterization was performed via (i) XRD studies at a Japan Rigaku D/max-rA X-ray diffractometer system with monochromatized Cu K α radiation ($\lambda = 1.5418 \text{ \AA}$), and (ii) SEM images obtained at a field emission scanning electron microscope (FE-SEM, Hitachi, S-4800). In the latter case a small drop of the sample re-dispersed in hexane was deposited on a silicon substrate and air-dried. The upconversion emission spectra were collected using a Jobin-Yvon LabRam Raman spectrometer system equipped with holographic gratings of 1800 and 600 grooves/mm and a Peltier air-cooled CCD detector. A 980 nm CW laser diode was used for optical excitation, and the beam was focused to a spot size of approximately 0.2 mm in diameter. The lifetimes of the $^4\text{S}_{3/2}$ and $^4\text{F}_{9/2}$ states of Er^{3+} were measured with (1) a 500 MHz Tektronix digital oscilloscope under excitation of 980 nm light pulses from an ns optical parametric oscillator, and (2) a Hamamatsu C5680-21 streak camera in combination with excitation around 960 nm provided by a dye laser.

3.3 Results and Discussion

In this experiment six $\alpha\text{-NaYF}_4\text{:Yb}^{3+},\text{Er}^{3+}@ \alpha\text{-NaYF}_4$ core/shell structure samples were synthesized. A schematic illustration of the structures of these six samples is given in **Scheme 3.1** (this scheme does not show Yb^{3+} doping ions). In these samples the $\alpha\text{-NaYF}_4\text{:Yb}^{3+},\text{Er}^{3+}$ cores remain of the same size. The only difference between them is the shell thickness, which was controlled during the shell-growing period. Compared to the other samples, samples **S5** and **S6** can not be dispersed in non-polar organic solvents in a stable manner. **Figure 3.1** shows the SEM images of the six samples. The average particle sizes are 8.8 nm (**S1**), 10.9 nm (**S2**), 12.8 nm (**S3**), 15.1 nm (**S4**), 17.5 nm (**S5**), and 20.0 nm (**S6**), respectively. As a reference, an SEM image of the bare core nanoparticle is also given in **Figure 3.1**. From this figure the size of the core is determined as 6.0 nm.



Scheme 3.1. Schematic illustration of the structure of the samples S1 to S6.

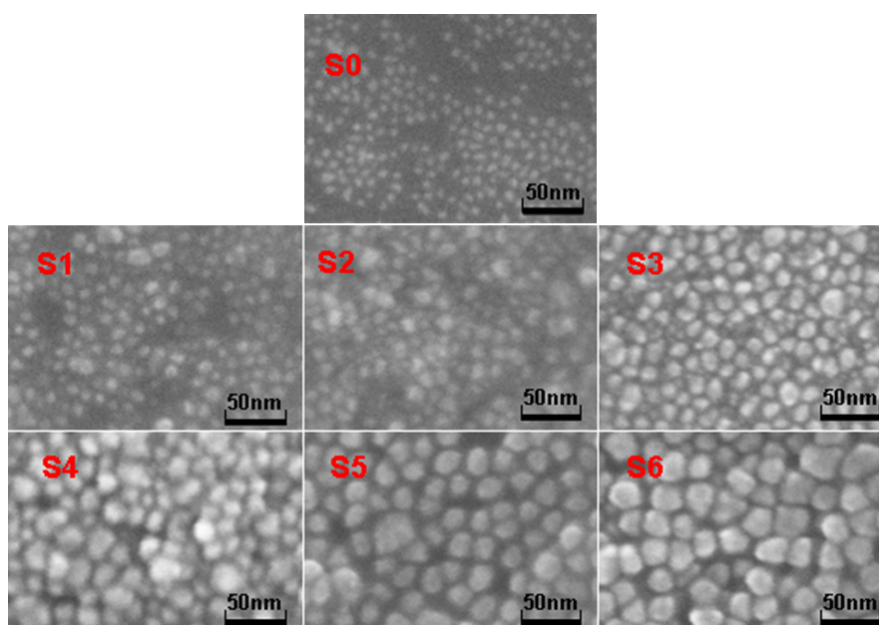


Figure 3.1. SEM images of S1, S2 up to S6; S0 are the naked core nanoparticles.

The powder X-ray diffraction (XRD) patterns of the samples displayed in **Figure 3.2** show well-defined peaks, indicating the high crystallinity of the synthesized nanoparticles of pure α -NaYF₄ referenced with the JCPDS card: 77-2042. Increasing the shell thickness, the X-ray diffraction peaks become sharper and sharper. From the line broadening of the diffraction peaks, the crystallite sizes of the six samples were determined to be approximately 9.1, 10.4, 12.5, 14.6, 16.3 and 18.5 nm using the Debye-Scherrer formula. These sizes are in agreement with the results obtained from the SEM images.

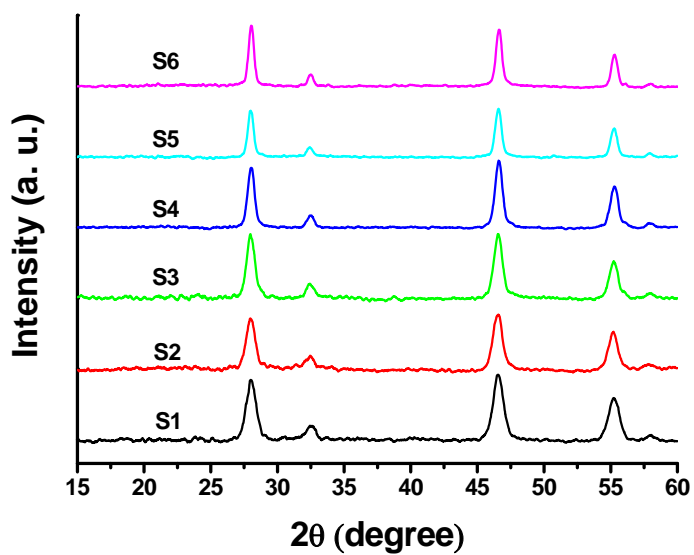


Figure 3.2. XRD patterns of samples of S1, S2 up to S6.

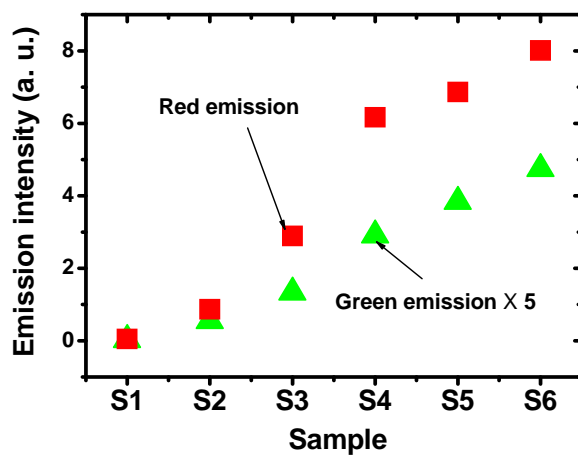


Figure 3.3. Green and red integrated upconversion emissions of the six samples under the excitation power density of about 60 W/cm^2 . The green emission band (520 - 560 nm) is enlarged by five times.

Chapter 3

The upconversion emission spectra of Er^{3+} ions in $\alpha\text{-NaYF}_4$ nanoparticles are shown in **Figure 3.3**. In these experiments an excitation wavelength of 980 nm is used with an excitation power density of about 60 W/cm^2 . Compared to **S1**, the upconversion emission intensity increases from 20 times (**S2**) to 160 times (**S6**). This trend can be rationalized by the fact that for small samples the surface area determines to a large extent the properties of the nanoparticle. For example, for nanoparticles of $\sim 6 \text{ nm}$ in size more than 60% of the crystal lattice is on the surface. This means that more than 60% of the rare earth ions are located in the surface thin layer. Here they are subject to nonradiative relaxation caused by surface defects and high-frequency vibrational modes of the coupled organic molecules, as a result of which the emission is quenched.

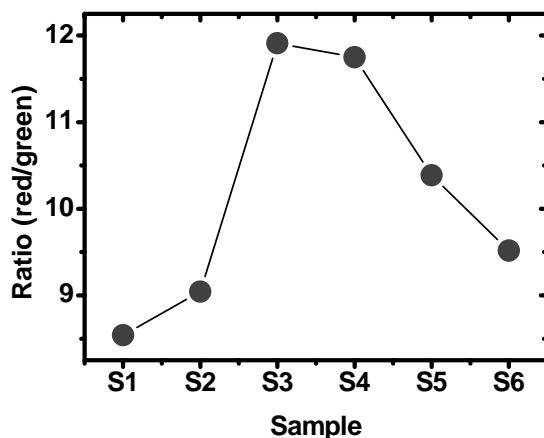


Figure 3.4. The intensity ratio of red/green of the six samples under IR excitation with the power density of 60 W/cm^2 .

Surprisingly, the shape of the emission spectrum does not change monotonically as a function of the shell thickness (**Figure 3.4**). In detail, the red to green emission ratio increases from 8.5 in **S1** to 12.0 in **S3**, and then decreases to 9.5 in **S6**. To understand this phenomenon, we have to consider the complex upconversion mechanism occurring in rare earth ions. In Er^{3+} , for example, several population routes co-exist for the $^4\text{F}_{9/2}$ level. In our previous work we showed that cross-relaxation can not be neglected when the Er^{3+} concentration is around 2%.^[3a] Strong cross-relaxation favors red emission. When the first layer of the homogeneous shell is grown on the surface of the nanoparticles, a significant amount of nonradiative centers located on the surface of $\text{NaYF}_4:\text{Yb}^{3+},\text{Er}^{3+}$ nanoparticles

are eliminated due to the shielding effect of the NaYF₄ shell. Cross-relaxation processes will be enhanced resulting in the increase of the red to green emission ratio. The process described above is defined as the first stage. When the shell continues to grow in the second stage, the surface and emission centers will be spatially more and more separated. This will weaken the interaction between high-frequency vibrational modes and optical transitions in emissive ions and thus decrease the red emission. As a result, the red to green emission ratio is reduced as observed at the second stage.

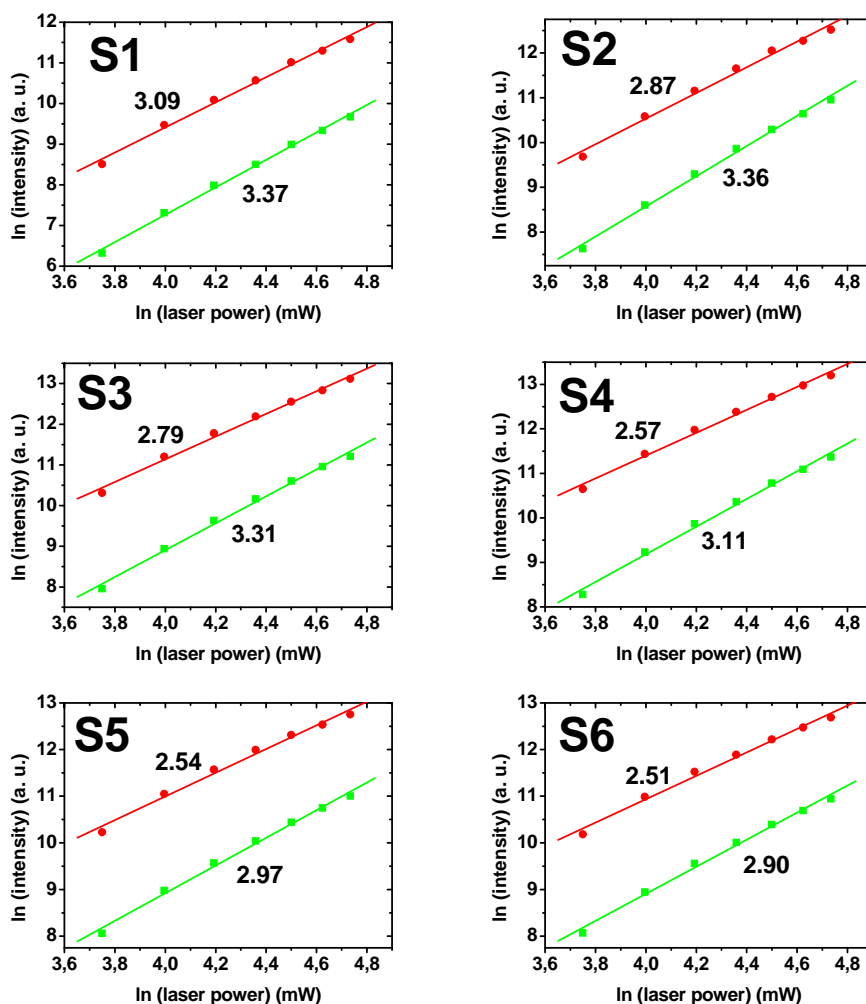


Figure 3.5. Logarithmic plots of the integrated intensity of the upconversion emission from level $^2H_{11/2}/^4S_{3/2}$ and $^4F_{9/2}$ to $^4I_{15/2}$ obtained under 980 nm laser excitation.

Chapter 3

Considering the upconversion mechanism (excited-state absorption (ESA) or energy-transfer upconversion (ETU)) the intensity of the visible output will be proportional to some power (n) of the infrared excitation power. **Figure 3.5** shows that in our experiments n varies from 3.37 to 2.90 for red emission and from 3.09 to 2.51 for green emission with the increase of the shell thickness. For processes involving only ESA and/or ETU n should not exceed 2. We thus conclude that other processes are involved as well. Considering the relatively high doping concentration of Er^{3+} (2 mol %) cross relaxation (${}^2\text{H}_{11/2} \rightarrow {}^4\text{F}_{9/2}$ vs. ${}^4\text{I}_{11/2} \rightarrow {}^4\text{F}_{9/2}$) should occur here,^[5] which would lead to values of n larger than 2.

Population of ${}^4\text{F}_{7/2}$ from a three-photon populated energy level (${}^4\text{G}_{11/2}$) might be another reason that n exceeds 2. This explanation is, however, at odds with the observation that upon increasing the shell thickness in the core/shell structure n gets closer to 2. When the shell thickness is increased, one expects that the influence of high-frequency vibrational modes of the surface organic groups would be reduced. Following this argument, the nonradiative relaxation efficiency should decrease when the shell gets thicker, which in turn should decrease nonradiative relaxation from ${}^4\text{G}_{11/2}$ to ${}^4\text{F}_{7/2}$ decreases. This will lead to a higher population of ${}^4\text{G}_{11/2}$ contributing to ultraviolet radiation, and a reduced contribution of emission from ${}^4\text{F}_{7/2}$ populated via nonradiative relaxation.

Both the green and red luminescence decay curves of the six samples are close to an exponential form, which means that all emission centers experience nearly the same local environment. The time evolution of the green (${}^4\text{S}_{3/2}$ - ${}^4\text{I}_{15/2}$) and red (${}^4\text{F}_{9/2}$ - ${}^4\text{I}_{15/2}$) upconversion luminescence of the six samples of core/shell nanoparticles with different shell thicknesses are depicted in **Figure 3.6**. All curves can be fitted well to the following equation with one rise and one decay component:

$$I(t) = -Ae^{-\frac{t}{\tau_r}} + Be^{-\frac{t}{\tau}}$$

where A , and B are all positive parameters. It has to be realized that a luminescence decay does not always represent the lifetime of the emissive energy level,^[9] and that a luminescence rise does not always represent the population of the emissive level as well. This is due to the fact that when a rise and a decay component co-exist in luminescence kinetics, the decay is always the longer one, even if the population rate is faster than the depopulation rate. Upconversion luminescence of rare earth ions is precisely one of these examples where the population rate is usually faster. The intermediate states, e.g. ${}^4\text{I}_{11/2}$ and ${}^4\text{I}_{13/2}$, that mediate the upconversion process have much longer lifetimes than the

upconversion emissive states, e.g. $^4S_{3/2}$ (for green emission) and $^4F_{9/2}$ (for red emission). The rise components in our measurements are determined by the lifetimes of the latter states, whereas the intermediate states determine to a large extent the decay components of the upconversion luminescence kinetics. Therefore the rise constant reflects mainly the nature of $^4I_{11/2}$ states in green emission and $^4I_{13/2}$ states in red emission, and the decay constant represents the lifetime of the $^4S_{3/2}$ or $^4F_{9/2}$ states.

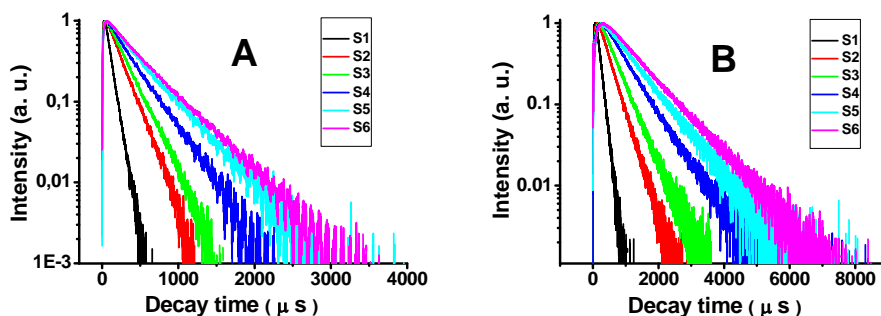


Figure 3.6. Temporal behavior of the green (A) and red (B) upconversion luminescence of the series of core/shell structure nanoparticles.

Table 3.1. Rise and decay components of the green and red emission of core/shell nanoparticles with different shell thickness.

	Green emission (545 nm)		Red emission (660 nm)	
	τ_r (μ s)	τ (μ s)	τ_r (μ s)	τ (μ s)
S 1	8	73	40	113
S 2	10	168	50	327
S 3	13	200	78	440
S 4	13	290	93	672
S 5	13	345	106	850
S 6	13	350	110	990

From **Table 3.1** it can be seen that for both the green and red emission the upconversion luminescence decay lifetime increases with the shell thickness. The same is true for the rise time of the red emission. The rise time of the green emission, however, remains constant after sample **S3**, which indicates that the previously mentioned

Chapter 3

surface-related effects can be neglected when considering the vibrational relaxation dynamics of the ${}^4I_{11/2}$ state.

To elucidate further the effects of the surface, the optical properties of UCNPs with different surface ligands were studied. Two samples were prepared. A NaYF_4 : 20% Yb^{3+} , 2% Er^{3+} UCNPs (core) powder sample with oleylamine (OM) ligands was synthesized. Part of these UCNPs was transferred to the hydrophilic phase by substitution of the OM ligands with the 2-aminoethyl dihydrogenphosphate (AEP) ligand via a ligand exchange process. We measured the upconversion lifetime of the green (${}^4S_{3/2}$ - ${}^4I_{15/2}$) and red (${}^4F_{9/2}$ - ${}^4I_{15/2}$) transitions of the two samples with different surface ligands of which the time-resolved emission spectra are depicted in **Figure 3.7**. **Table 3.2** reports the time constants obtained from fitting the luminescence decay curves for the red and green emissions of the two samples. We observe that both green and red emissions are quenched to a larger extent than observed for the sample with OM ligands, which can be rationalized by the fact that the AEP ligands contain more -OH, - NH_2 high vibrational energy modes.

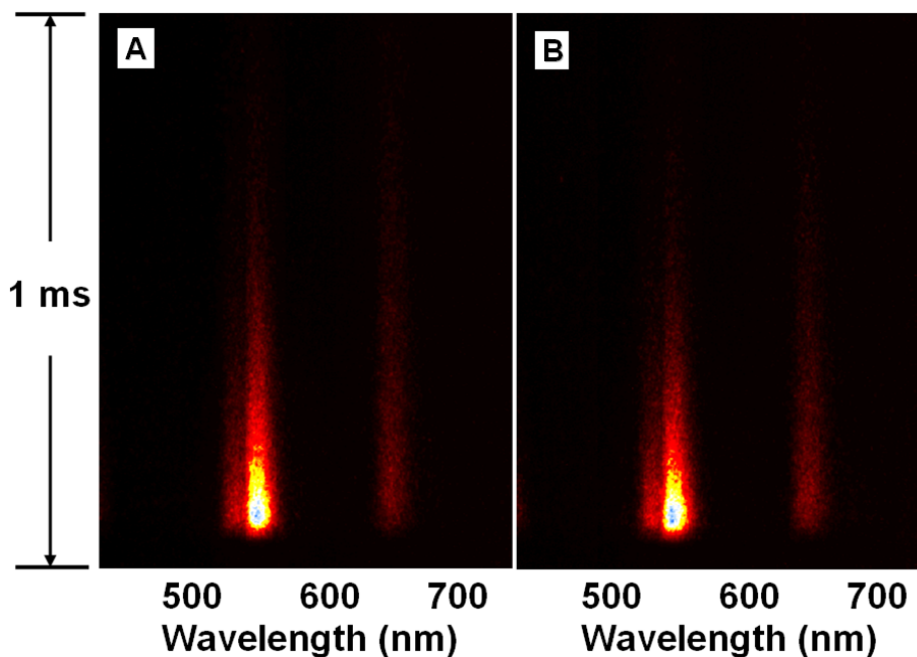


Figure 3.7. Streak image of time-resolved upconversion luminescence spectra of UCNPs with OM (A) and AEP (B) ligands on the surface ($\lambda_{exc} = 950\text{nm}$).

Table 3.2. Rise and decay components of the green and red emission of core/shell nanoparticles with different shell thicknesses.

	UCNPs-OM		UCNPs-AEP	
	545 emission	660 emission	545 emission	660 emission
Rise (μ s)	10.4	29.1	9.4	22.1
Decay (μ s)	137.9	269.4	114.2	209.9

3.4 Conclusions

From an analysis of the luminescence kinetics of core/shell UCNPs it has become clear that generally a large number of luminescent centers of the core nanoparticle are severely quenched, but can be recovered by homogeneous coating. Our results demonstrate that the surface-related high-frequency vibrational modes play an important role in the upconversion process. Coating a homogenous shell can alter the upconversion channels and thus be used to manipulate the upconversion mechanism and control the upconversion luminescence spectra.

3.5 Acknowledgements

This work was supported by NSFC of China (60771051, 60601015, 10674132, 10874179 and 20603035), and the exchange program between CAS of China and KNAW of the Netherlands.

3.6 References:

- (a) NaYF₄ : Yb,Er—an Efficient Upconversion Phosphor. N. Menyuk, K. Dwight, and F. Pinaud; *Appl. Phys. Lett.*, **1972**, *21*, 159; (b) Phosphors for the Conversion of Infrared Radiation into Visible Light. J.L. Sommerdijk, A. Bril; *Philips Tech. Rev.*, **1974**, *34*, 1.
- (a) Up-Converting Phosphor Reporters for Nucleic Acid Microarrays. F. van de Rijke, H. Zijlmans, S. Li, T. Vail, A.K. Raap, R.S. Niedbala, and H.J. Tanke; *Nat. Biotechnol.*, **2001**, *19*, 273-276; (b) In Vivo and Scanning Electron Microscopy Imaging of Upconverting Nanophosphors in *Caenorhabditis elegans*. S.F. Lim, R. Riehn, W.S. Ryu, N. Khanarian, C.K. Tung, D. Tank, and R.H. Austin; *Nano Lett.*, **2006**, *6*, 169-174. (c) Green Upconversion Nanocrystals for DNA detection. L.Y. Wang, and Y.D. Li; *Chem.*

- Commun.*, **2006**, *24*, 2557-2559; (d) Versatile Photosensitizers for Photodynamic Therapy at Infrared Excitation. P. Zhang, W. Steelant, M. Kumar, and M. Scholfield; *J. Am. Chem. Soc.*, **2007**, *129*, 4526-4527; (e) Design of a Highly Sensitive and Specific Nucleotide Sensor Based on Photon Upconverting Particles. P. Zhang, S. Rogelj, K. Nguyen, and D. Wheeler; *J. Am. Chem. Soc.*, **2006**, *128*, 12410-12411; (f) High Contrast in Vitro and in Vivo Photoluminescence Bioimaging Using Near Infrared to Near Infrared Up-Conversion in Tm³⁺ and Yb³⁺ Doped Fluoride Nanophosphors. M. Nyk, R. Kumar, T.Y. Ohulchansky, E.J. Bergey, and P.N. Prasad; *Nano Lett.*, **2008**, *8*, 3834-3838.
- 3 (a) Upconversion Luminescence of β -NaYF₄: Yb³⁺, Er³⁺@ β -NaYF₄ Core/Shell Nanoparticles: Excitation Power Density and Surface Dependence. Y. Wang, L.P. Tu, J.W. Zhao, Y.J. Sun, X.G. Kong, and H. Zhang; *J. Phys. Chem. C*, **2009**, *113*, 7164-7169; (b) A Facile Synthesis and Photoluminescent Properties of Redispersible CeF₃, CeF₃:Tb³⁺, and CeF₃:Tb³⁺/LaF₃ (Core/Shell) Nanoparticles. Z.L. Wang, Z.W. Quan, P.Y. Jia, C.K. Lin, Y. Luo, Y. Chen, J. Fang, W. Zhou, C.J. O'Connor, J. Lin; *Chem. Mater.*, **2006**, *18*, 2030-2037; (c) Epitaxial Synthesis of Uniform Cerium Phosphate One-Dimensional Nanocable Heterostructures with Improved Luminescence. W.B. Bu, Z.L. Hua, H.R. Chen, and J.L. Shi; *J. Phys. Chem. B*, **2005**, *109*, 14461-14464; (d) Synthesis of Eu³⁺-Doped Core and Core/Shell Nanoparticles and Direct Spectroscopic Identification of Dopant Sites at the Surface and in the Interior of the Particles. O. Lehmann, K. Kömpe, and M. Haase; *J. Am. Chem. Soc.*, **2004**, *126*, 14935-14942; (e) Surface Modification of ZrO₂:Er³⁺ Nanoparticles to Attenuate Aggregation and Enhance Upconversion Fluorescence. Q.Lü, F.Y. Guo, L. Sun, A.H. Li, and L.C. Zhao; *J. Phys. Chem. C*, **2008**, *112*, 2836-2844; (f) LaF₃, CeF₃, CeF₃:Tb³⁺, and CeF₃:Tb³⁺@LaF₃ (Core-Shell) Nanoplates: Hydrothermal Synthesis and Luminescence Properties. C.X. Li, X.M. Liu, P.P. Yang, C.M. Zhang, H.Z. Lian, and J. Lin; *J. Phys. Chem. C*, **2008**, *112*, 2904-2910; (g) Effects of the Coating Process on Nanoscale Y₂O₃:Eu³⁺ Powders. Q. Li, L. Gao, and D.S. Yan; *Chem. Mater.*, **1999**, *11*, 533-535; (h) Luminescence Enhancement by Energy Transfer in Core-Shell Structures. C. Louis, S. Roux; G. Ledoux, C. Dujardin, O. Tillement, B.L. Cheng, and P. Perriat; *Chem. Phys. Lett.*, **2006**, *429*, 157-160; (i) Luminescent Enhancement in Europium-doped Yttria Nanotubes Coated with Yttria. X. Bai, H.W. Song, G.H. Pan, Z.X. Liu, S.Z. Lu, W.H. Di, X.G. Ren, Y.Q. Lei, Q.L. Dai, and L.B. Fan; *Appl. Phys. Lett.*, **2006**, *88*, 143104; (j) Facile Sonochemical Synthesis of CePO₄:Tb/LaPO₄ Core/shell Nanorods with Highly Improved Photoluminescent Properties. L. Zhu, X.M. Liu, X.D. Liu, Q. Li, J.Y. Li, S.Y. Zhang, J. Meng, and X.Q. Cao; *Nanotechnology*, **2006**, *17*, 4217; (k) Green-Emitting CePO₄:Tb/LaPO₄ Core-Shell Nanoparticles with 70% Photoluminescence Quantum Yield. K. Kömpe, H. Borchert, J. Storz, A. Lobo, S. Adam, T. Möller, and M. Haase; *Angew. Chem., Int. Ed.*, **2003**, *42*, 5513-5516.; (l) Water-Soluble NaYF₄:Yb,Er(Tm)/

-
- NaYF₄/Polymer Core/Shell/Shell Nanoparticles with Significant Enhancement of Upconversion Fluorescence. G.S. Yi, and G.M. Chow; *Chem. Mater.*, **2007**, *19*, 341-343.
- 4 (a) Synthesis of Colloidal Upconverting NaYF₄ Nanocrystals Doped with Er³⁺, Yb³⁺ and Tm³⁺, Yb³⁺ via Thermal Decomposition of Lanthanide Trifluoroacetate Precursors. J.C. Boyer, F. Vetrone, L.A. Cuccia, and J.A. Capobianco; *J. Am. Chem. Soc.*, **2006**, *128*, 7444-7445; (b) Improvement in the Luminescence Properties and Processability of LaF₃/Ln and LaPO₄/Ln Nanoparticles by Surface Modification. J.W. Stouwdam, and F.C.J.M. van Veggel; *Langmuir*, **2004**, *20*, 11763-11771; (c) Synthesis of Hexagonal-Phase NaYF₄:Yb,Er and NaYF₄:Yb,Tm Nanocrystals with Efficient Up-Conversion Fluorescence. G.S. Yi, and G.M. Chow; *Adv. Funct. Mater.*, **2006**, *16*, 2324-2329.
- 5 Tunable Red-Green Upconversion Luminescence in Novel Transparent Glass Ceramics Containing Er: NaYF₄ Nanocrystals. F. Liu, E. Ma, D.Q. Chen, Y.L. Yu, and Y.S. Wang; *J. Phys. Chem. B*, **2006**, *110*, 20843-20846.